2019-01

A tip-tilt hardware-in-the-loop air-bearing test bed with physical emulation of the relative orbital dynamics

Ogundele, Ayansola D.; Fernandez, Bautista R.; Virgili-Llop, Josep; Romano, Marcello

AAS

Ogundele, Ayansola D., et al. "A tip-tilt hardware-in-the-loop air-bearing test bed with physical emulation of the relative orbital dynamics." Adv Astronaut Sci 168.2019 (2019): 3781-3799.
http://hdl.handle.net/10945/70603

AAS 19-511

A TIP-TILT HARDWARE-IN-THE-LOOP AIR-BEARING TEST BED WITH PHYSICAL EMULATION OF THE RELATIVE ORBITAL DYNAMICS

Ayansola D. Ogundele[*], Bautista R. Fernandez[†], Josep Virgili-Llop[‡], Marcello Romano[§]

A new hardware-in-the-loop (HIL) air bearing testbed that is capable of physically emulating the relative orbital dynamics is presented. Typically, air bearing testbeds consist of test vehicles operating on top of a planar and horizontally-leveled surface. These test vehicles use air bearings to reduce the friction with the operating surface to negligible levels. The low friction, combined with the horizontally-leveled surface, creates a low residual acceleration environment. These dynamics are representative of the environment that spacecraft experience during close proximity maneuvers. To extend the applicability of planar air bearing test beds to longer maneuvers or separations relative orbital dynamics need to be emulated. In this paper, using Hill-Clohessy-Wilshire dynamics, we emulated the relative orbital dynamics of a real spacecraft using a scaled Floating Spacecraft Simulator (FSS) on a dynamically inclined operating surface. The mathematical constructs of the tilt angles, screw height displacements and scaling parameters are developed via Euler's rotation theorem, Buckingham's Pi theorem and the similarity principle. The applicability of the new idea is demonstrated via a circumnavigation maneuver scenario of a spacecraft in a Low Earth Orbit (LEO). The simulation results show the viability and suitability of the new approach.

INTRODUCTION

In recent years, the Hardware-in-the-Loop Testbed (HILT) has gained tremendous attentions from the aerospace, defense industries, marine and automobile researchers due to the numerous advantages it offers. The HILT, commonly used to carry out laboratory experiments, is less costly because it requires less hardware than fully physical prototypes, the simulators are easy to build and can achieve fidelity levels unattainable through purely virtual simulation. In addition, the testbed can be used to train personel such as satellite operators, airplane pilots and flight simulators.[1]

The surge in interest on spacecraft formation flying, involving the use of smaller spacecraft to perform tasks that can be carried out by a single large spacecraft, has necessitated the need to better understand the orbital dynamics of each of the spacecraft in the formation. The formation can be

[*]NRC Research Associate, Spacecraft Robotics Laboratory, Department of Mechanical and Aerospace Engineering, Naval Postgraduate School, 1 University Circle, Monterey, CA.

[†]Faculty Associate,Adaptive Optics Center of Excellence, Spacecraft Research and Design Center, Department of Mechanical and Aerospace Engineering, Naval Postgraduate School, 1 University Circle, Monterey, CA.

[‡]NRC Research Associate, Spacecraft Robotics Laboratory, Department of Mechanical and Aerospace Engineering, Naval Postgraduate School, 1 University Circle, Monterey, CA.

[§]Professor, Spacecraft Robotics Laboratory, Department of Mechanical and Aerospace Engineering, Naval Postgraduate School, 1 University Circle, Monterey, CA.

used in astronomy, earth science, to form radio-telescope, surface mapping array, synthetic aperture radar, etc.[2–6] Generally, Hill-Clohessy-Wilshire (HCW) linearized equations of motion[7,8]

$$\begin{aligned} \ddot{x} - 2\omega\dot{y} - 3\omega^2 x &= 0 \\ \ddot{y} + 2\omega\dot{x} &= 0 \\ \ddot{z} + \omega^2 z &= 0 \end{aligned} \tag{1}$$

derived using Local Vertical Local Horizontal (LVLH) rotating frame of the chief spacecraft with the mean motion $\omega = \sqrt{\mu/R^3}$, where R is the orbital radius of the chief spacecraft, are used to determine the relative motion of a deputy spacecraft with respect to the chief spacecraft. The equations were developed with the assumptions that the chief spacecraft is located in a circular orbit with no perturbation forces and Earth is spherical. The equations can be used to establish a large family of relative orbits that needed only small amount of fuel to maintain.[2]

Due to the stringent requirements of spacecraft formation flying and the need to better understand the relative motion dynamics, guidance, navigation and control, HIL air bearing testbeds which have low cost in comparison to the real physical system and of high reliability are used to investigate and emulate the dynamical behavior of the system. The air bearing testbeds consist of test vehicles that float on top of a planar and horizontally leveled surface through the air bearings to reduce the friction with the operating surface to negligible levels. The low friction, combined with the horizontally-leveled surface, creates a low residual acceleration environment. These dynamics are considered to be representative of the environment that spacecraft experience during close proximity maneuvers. Given their dynamic fidelity, this type of testbeds have been widely adopted.[9–16] However, as the relative orbital dynamics are not emulated, these testbeds are limited to reproduce short maneuvers where the vehicles are in very close proximity of each other. To extend the applicability of planar air bearing testbeds to longer maneuvers or separations the relative orbital dynamics need to be emulated. Previously it has been proposed to use the test vehicle's actuators to impart these accelerations.[17] However, using the vehicles actuators to generate this natural motion interferes in a non-realistic way with the vehicle's own maneuvering.

Brief survey of the planar testbeds is given as follows. NASA Goddard Space Flight Centers (GSFCs) Guidance, Navigation, and Control (GNC) Center developed Formation Flying Testbed (FFTB), a modular, hybrid dynamic simulation facility for end-to-end guidance, navigation, and control analysis and design for formation flying clusters and constellations of satellites.[9] To demonstrate a formation flying control system for the Terrestrial Planet Finder Interferometer (TPF-I) NASA Jet Propulsion Laboratory (JPL) developed Formation Control Testbed (FCT)[10] and in order to test GNC formation flying algorithms German Aerospace Center (DLR) developed Test Environment for Applications of Multiple Spacecraft (TEAMS).[11] At Naval Postgraduate School (NPS), Spacecraft Robotics Laboratory (SRL) developed a fourth generation testbed named the Proximity Operation of Spacecraft: Experimental hardware-In-the-loop DYNamic (POSEIDYN) simulator and through experiment tested algorithms for autonomous rendezvous and proximity operations.[12] The ADvanced Autonomous MUltiple Spacecraft (ADAMUS) testbed,[13] a 6-DOF simulator, was developed at the University of Florida and Georgia Tech developed 5-DOF Autonomous Spacecraft Testing of Robotic Operations in Space (ASTROS) testbed.[14] At the Astrodynamics and Control Laboratory (ACL) of Yonsei University the Autonomous Spacecraft Test Environment for Rendezvous In proXimity (ASTERIX) facility was developed to provide a space-representative environment to experimentally evaluate GNC algorithms for proximity operation and formation flying.[15]

This paper describes in detail the design and development of a new hardware-in-the-loop air

bearing testbed that has the ability to physically emulate the relative orbital dynamics. In order to extend the applicability of the planar air bearing testbeds a new approach that involves dynamical changing of the inclination of the operating surface for a better physical emulation of the relative orbital dynamics is presented. A prototype implementation of the approach has been described with a maneuver example to demonstrate the effectiveness of the prototype.

DIRECTION COSINE MATRIX FOR SCREW HEIGHT DISPLACEMENTS

In this section, we present mathematical constructs of the Euler axes created by two successive rotations of the Mechanical Screw Actuator (MSA) and the Direction Cosine Matrix (DCM). From these the screw height displacements are formulated. The planar testbed has two-degrees-of-freedom requiring two coordinates, x and y, to describe its motion. As shown in Figure 1, the granite table is supported by a bolt at point P_0 and two MSAs at points P_1 and P_2.

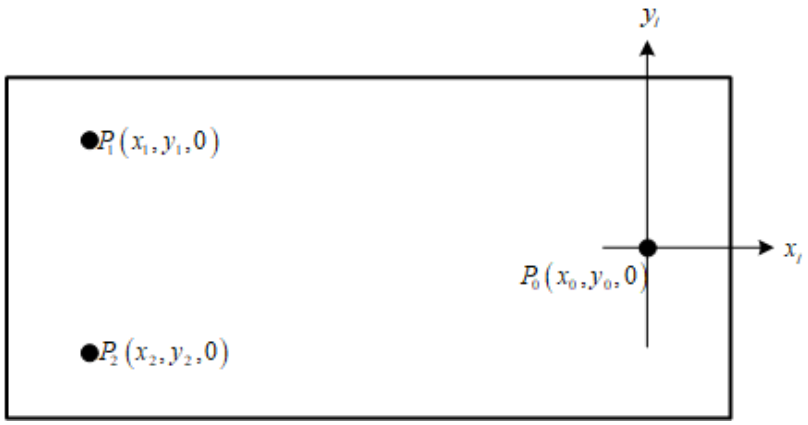

Figure 1. Granite table on three points of support P_0, P_1 and P_2 in horizontal configuration.

Rotation of the granite due to vertical displacements of points P_1 and P_2

The classical Eulers theorem, which utilizes only one special angle (i.e., Euler rotation angle θ) to quantify the relative rotation between two frames and only one special vector (i.e., Euler axis ε) to define the central axis of the rotation, is employed to express the rotation of the granite due to vertical displacements of P_1 and P_2. This is based on the general displacement of a rigid body with one fixed point which is a rotation about an axis through that point.[18,19] In our case the fixed point is P_0. The displacement of the heights based on the concept of Euler angle and axis is formulated using the DCM[18]

$$\mathbf{C} = \cos\theta\mathbf{I} + (1 - \cos\theta)\,\varepsilon\varepsilon^T - \sin\theta\varepsilon^\times \tag{2}$$

where,

$$\varepsilon = \begin{bmatrix} \varepsilon_1 \\ \varepsilon_2 \\ \varepsilon_3 \end{bmatrix}, \quad \mathbf{I} = \begin{bmatrix} 1 & 0 & 0 \\ 0 & 1 & 0 \\ 0 & 0 & 1 \end{bmatrix}, \quad \varepsilon^\times = \begin{bmatrix} 0 & -\varepsilon_3 & \varepsilon_2 \\ \varepsilon_3 & 0 & -\varepsilon_1 \\ -\varepsilon_2 & \varepsilon_1 & 0 \end{bmatrix} \tag{3}$$

Eq. (2) can be rewritten as

$$\mathbf{C} = \begin{bmatrix} \mathrm{c}\theta + \varepsilon_1^2(1-\mathrm{c}\theta) & \varepsilon_1\varepsilon_2(1-\mathrm{c}\theta) + \varepsilon_3 s\theta & \varepsilon_1\varepsilon_3(1-\mathrm{c}\theta) - \varepsilon_2 s\theta \\ \varepsilon_2\varepsilon_1(1-\mathrm{c}\theta) - \varepsilon_3 s\theta & \mathrm{c}\theta + \varepsilon_2^2(1-\mathrm{c}\theta) & \varepsilon_2\varepsilon_3(1-\mathrm{c}\theta) + \varepsilon_1 s\theta \\ \varepsilon_3\varepsilon_1(1-\mathrm{c}\theta) + \varepsilon_2 s\theta & \varepsilon_3\varepsilon_2(1-\mathrm{c}\theta) - \varepsilon_1 s\theta & \mathrm{c}\theta + \varepsilon_3^2(1-\mathrm{c}\theta) \end{bmatrix} \tag{4}$$

Here, $\cos\theta = c\theta$ and $\sin\theta = s\theta$.

Rotation about axis P_0P_2: The first rotation, carried out to dynamically recreate the orbital dynamics, is done by actuating the MSA located at point P_1 as shown in Figure 2. This leads to a rotation about Euler axis $\hat{\varepsilon}_2$, consisting of the straight line l_2 passing through points P_0 and P_2, by an angle θ.

$$\hat{\varepsilon}_2 = \frac{\overline{P_0P_2}}{|\overline{P_0P_2}|} = \varepsilon_1\hat{i} + \varepsilon_2\hat{j}, \quad \varepsilon_1 = \frac{x_2}{l_2}, \quad \varepsilon_2 = \frac{y_2}{l_2}, \quad \sin\theta = \frac{z_1}{d_1}, \quad l_1 = \sqrt{x_1^2 + y_1^2}, \quad l_2 = \sqrt{x_2^2 + y_2^2} \tag{5}$$

After the rotation P_1 becomes P_1' with coordinates (x_1', y_1', z_1) where z_1 represents the displacement of the screw height at P_1.

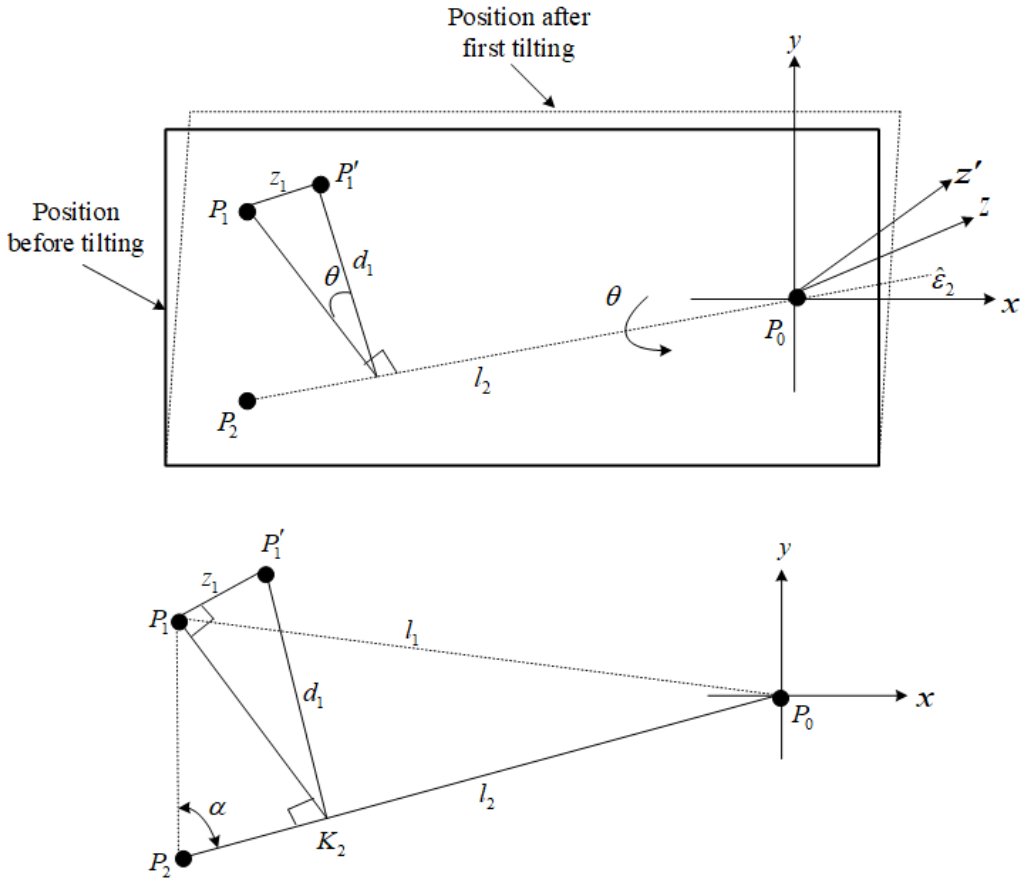

Figure 2. Granite table position before and after rotation of MSA at P_1.

Applying cosine rule to triangle $P_1P_2P_0$ we have

$$\cos\alpha = \frac{x_2^2 + y_2^2 - x_1x_2 - y_1y_2}{\sqrt{\left\{(x_1 - x_2)^2 + (y_1 - y_2)^2\right\}\left(x_2^2 + y_2^2\right)}} \tag{6}$$

Solving for d_1 yields

$$d_1 = \sqrt{z_1^2 + \left\{(x_1 - x_2)^2 + (y_1 - y_2)^2\right\}\sin^2\alpha} \tag{7}$$

and using small angle approximation, where $z_1^2 \approx 0$, reduces Eq. (7) to

$$d_1 = \left(\sqrt{(x_1 - x_2)^2 + (y_1 - y_2)^2}\right)\sin\alpha \tag{8}$$

Assuming there is a small rotation of angle,

$$\sin\theta = \theta \approx \tfrac{z_1}{d_1}, \quad \cos\theta \approx 1, \quad x'_1 \approx x_1, \quad y'_1 \approx y_1 \tag{9}$$

Substituting Eq. (6) into Eq. (4) gives

$$\mathbf{C}_1(x_1, y_1, z_1, x_2, y_2, z_2) = \begin{bmatrix} 1 & \varepsilon_3\theta & -\varepsilon_2\theta \\ -\varepsilon_3\theta & 1 & \varepsilon_1\theta \\ \varepsilon_2\theta & -\varepsilon_1\theta & 1 \end{bmatrix} \approx \begin{bmatrix} 1 & 0 & -\frac{y_2z_1}{l_2d_1} \\ 0 & 1 & \frac{x_2z_1}{l_2d_1} \\ \frac{y_2z_1}{l_2d_1} & -\frac{x_2z_1}{l_2d_1} & 1 \end{bmatrix} \tag{10}$$

and

$$\mathbf{P}'_1 = \mathbf{C}_1(x_1, y_1, z_1, x_2, y_2, z_2)\,\mathbf{P}_1 \tag{11}$$

Rotation about axis P_0P_1: Performing second rotation by actuating MSA at P_2 implies rotation about Euler axis 1, $\hat{\varepsilon}_1$, consisting of a straight line l_1 passing through points P_0 and P_1, by angle β as shown in Figure 3.

$$\hat{\varepsilon}_1 = \frac{\overline{P_0P_1}}{|\overline{P_0P_1}|} = \varepsilon_1\hat{i}' + \varepsilon_2\hat{j}', \quad \varepsilon_1 = \tfrac{x_1}{l_1}, \quad \varepsilon_2 = \tfrac{y_1}{l_1}, \quad \sin\beta = \tfrac{z_2}{d_2} \tag{12}$$

The second rotation changes P_2 to P'_2 having coordinates (x'_2, y'_2, z_2) where z_2 represents the second displacement of the second screw height.

Applying cosine rule to triangle $P_1P_0P_2$ we have

$$\cos\gamma = \frac{x_1x_2 + y_1y_2}{\sqrt{\left(x_1^2 + y_1^2\right)\left(x_2^2 + y_2^2\right)}} \tag{13}$$

Solving for d_2, using small angle approximation in which $z_2^2 \approx 0$, then

$$d_2 = \left(\sqrt{x_2^2 + y_2^2}\right)\sin\gamma \tag{14}$$

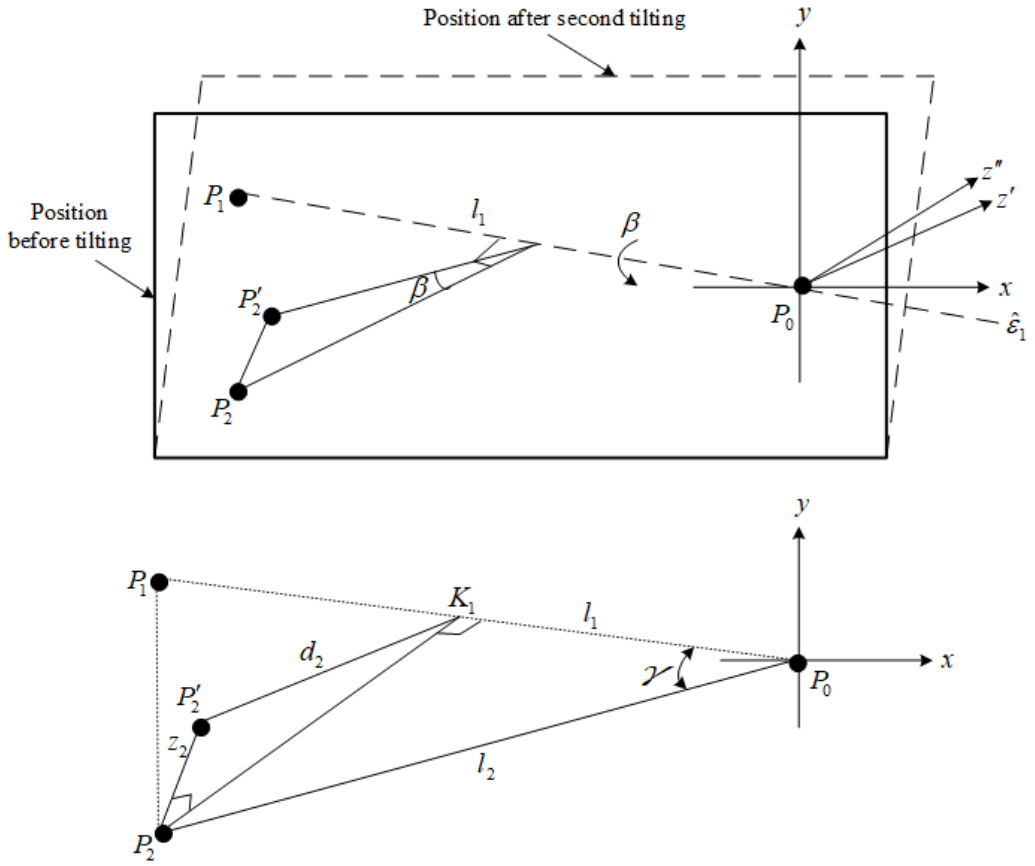

Figure 3. Granite table position before and after rotation of MSA at P_1.

With small angle approximation

$$\sin\beta = \beta \approx \tfrac{z_2}{d_2}, \quad \cos\beta \approx 1, \quad x'_2 \approx x_2, \quad y'_2 \approx y_2 \tag{15}$$

Upon substitution of Eq. (15) into Eq. (4) gives

$$\mathbf{C}_2\left(x_1, y_1, z_1, x_2, y_2, z_2\right) = \begin{bmatrix} 1 & \varepsilon_3\beta & -\varepsilon_2\beta \\ -\varepsilon_3\beta & 1 & \varepsilon_1\beta \\ \varepsilon_2\beta & -\varepsilon_1\beta & 1 \end{bmatrix} \approx \begin{bmatrix} 1 & 0 & -\frac{y_1 z_2}{l_1 d_2} \\ 0 & 1 & \frac{x_1 z_2}{l_1 d_2} \\ \frac{y_1 z_2}{l_1 d_2} & -\frac{x_1 z_2}{l_1 d_2} & 1 \end{bmatrix} \tag{16}$$

and

$$\mathbf{P}_2{}' = \mathbf{C}_1\left(x_1, y_1, z_1, x_2, y_2, z_2\right)\mathbf{P}_2 \tag{17}$$

Formulation of Screw Height Displacements

The screw height displacements at P_1 and P_2 are formulated using the composition of the two rotations derived in the last section. From Eqs. (10) and (16) the compound rotation matrix is

$$\mathbf{C}\left(x_1, y_1, z_1, x_2, y_2, z_2\right) = \mathbf{C}_2\left(x_1, y_1, z_1, x_2, y_2, z_2\right)\mathbf{C}_1\left(x_1, y_1, z_1, x_2, y_2, z_2\right) \tag{18}$$

This simplifies to

$$\mathbf{C}\left(x_1, y_1, z_1, x_2, y_2, z_2\right) = \begin{bmatrix} 1 - \frac{y_1 y_2 z_1 z_2}{l_1 l_2 d_1 d_2} & \frac{y_1 x_2 z_1 z_2}{l_1 l_2 d_1 d_2} & -\frac{y_2 z_1}{l_2 d_1} - \frac{y_1 z_2}{l_1 d_2} \\ \frac{x_1 y_2 z_1 z_2}{l_1 l_2 d_1 d_2} & 1 - \frac{x_1 x_2 z_1 z_2}{l_1 l_2 d_1 d_2} & \frac{x_2 z_1}{l_2 d_1} + \frac{x_1 z_2}{l_1 d_2} \\ \frac{y_1 z_2}{l_1 d_2} + \frac{y_2 z_1}{l_2 d_1} & -\frac{x_1 z_2}{l_1 d_2} - \frac{x_2 z_1}{l_2 d_1} & -\frac{y_1 y_2 z_1 z_2}{l_1 l_2 d_1 d_2} - \frac{x_1 x_2 z_1 z_2}{l_1 l_2 d_1 d_2} + 1 \end{bmatrix} \tag{19}$$

Taking cross product of $\mathbf{P}_1{}' = x_1\hat{i} + y_1\hat{j} + z_1\hat{k}$ and $\mathbf{P}_2{}' = x_2\hat{i} + y_2\hat{j} + z_2\hat{k}$ we have the normal and unit normal vectors projected in inertial frame as

$$\mathbf{n}^{\{I\}} = \mathbf{P}_1{}' \times \mathbf{P}_2{}' = \begin{bmatrix} y_2 z_1 - y_1 z_2 \\ x_1 z_2 - x_2 z_1 \\ x_2 y_1 - x_1 y_2 \end{bmatrix}, \qquad \hat{\mathbf{n}}^{\{I\}} = \frac{\mathbf{n}^{\{I\}}}{\left|\mathbf{n}^{\{I\}}\right|} \tag{20}$$

After two successive rotations the normal vector projected in the body frame becomes

$$\mathbf{n}^{\{B\}} = \mathbf{C}\left(x_1, y_1, z_1, x_2, y_2, z_2\right)\mathbf{n}^{\{I\}}, \qquad \hat{\mathbf{n}}^{\{B\}} = \mathbf{C}\left(x_1, y_1, z_1, x_2, y_2, z_2\right)\hat{\mathbf{n}}^{\{I\}} = \begin{bmatrix} 0 \\ 0 \\ 1 \end{bmatrix} \tag{21}$$

Consider a gravitational force $\mathbf{f}$ acting on the granite table before the rotation

$$\mathbf{f}^{\{I\}} = -mg\hat{\mathbf{n}}^{\{I\}} \tag{22}$$

After the first and second rotation of the two MSAs, the force in the body frames can be expressed as

$$\mathbf{f}^{\{B\}} = \mathbf{C}\left(x_1, y_1, z_1, x_2, y_2, z_2\right)\mathbf{f}^{\{I\}} \tag{23}$$

Using Eq. (22) and the fact that $\mathbf{f}^{\{B\}} = m\mathbf{a}$ where $\mathbf{a}$ is the Floating Spacecraft Simulator acceleration we have

$$\mathbf{a}^{\{B\}} = -\frac{g}{\left|\hat{\mathbf{n}}^{\{B\}}\right|} \begin{bmatrix} -\frac{y_2 z_1}{l_2 d_1} - \frac{y_1 z_2}{l_1 d_2} \\ \frac{x_2 z_1}{l_2 d_1} + \frac{x_1 z_2}{l_1 d_2} \\ -\frac{y_1 y_2 z_1 z_2}{l_1 l_2 d_1 d_2} - \frac{x_1 x_2 z_1 z_2}{l_1 l_2 d_1 d_2} + 1 \end{bmatrix} \tag{24}$$

With the small angle approximation we have

$$z_1 z_2 \ll 1, z_1^2 \ll 1, z_2^2 \ll 1, z_1 z_2^2 \ll 1, z_2 z_1^2 \ll 1 \tag{25}$$

and

$$\mathbf{z} = -\frac{1}{g}\mathbf{A}^{-1}\mathbf{a}^{\{B\}} \tag{26}$$

where, the nonsingular matrix $\mathbf{A}$ and the screw height displacement $\mathbf{z}$ are

$$\mathbf{A} = \begin{bmatrix} -\frac{y_2}{l_2 d_1} & -\frac{y_1}{l_1 d_2} \\ \frac{x_2}{l_2 d_1} & \frac{x_1}{l_1 d_2} \end{bmatrix} \qquad \mathbf{z} = \begin{bmatrix} z_1 \\ z_2 \end{bmatrix} \tag{27}$$

Equation (26) is fed into the controller to determine the amount by which the motor should move the screw actuator so as to displace the granite table to the desired position.

ANALYSIS OF THE SCALED SPACECRAFT RELATIVE MOTION DYNAMICS VIA BUCKINGHAM'S PI-THEOREM AND SIMILARITY PRINCIPLE

The relative motion dynamics of the scaled spacecraft model, which is dynamically similar to the real spacecraft and can be used to analyze its principles of operation, is developed via the Buckingham's Pi theorem and the similarity principle. In this paper, the Floating Spacecraft Simulator developed at the Spacecraft Robotics Lab of NPS represents a small scale replica of the real spacecraft model such as International Space Station (ISS) etc. The FSS is used to dynamically recreate and predict the orbital dynamics experienced by the real spacecraft in orbit. Through the help of dimensional analysis, the relationship between the relative motion variables in terms of the dimensional parameters helps to develop the replication of the motion in a smaller scale.

Buckingham's Pi Theorem and Similarity Conditions

The Buckingham's Pi[20,21] theorem states that, if there are n variables in a problem and these variables contain m primary (independent) dimensions (for example mass (M), length (L), and time (T)) it can be reduced to a relationship between $p = n - k$ dimensionless parameters $\pi_1, ..., \pi_{n-k}$. The dimensionless π groups can be constructed by choosing m dimensionally-distinct scaling (repeating) variables and for each of the remaining $p = n - k$ scaling variables we can construct a non-dimensional π of the form

$$\pi = (\text{var}iable)\,(scale_1)^a (scale_2)^b (scale_3)^c ... \tag{28}$$

where, $a, b, c...$ are chosen in such a way as to make each π non-dimensional.

The similarities between the scaled and the real spacecraft model must be established after the determination of the π groups. Between the real and scaled model three types of similarity must exist, geometric, kinematic and dynamic. Geometric similarity exists when the ratio of all their corresponding linear dimensions are equal. The similarity of motion between the real and scaled model is referred to as kinematic similarity, where the ratios of their respective velocities and accelerations at the corresponding points are the same in magnitude but parallel in direction. The dynamic similarity is between the models, referred to as dynamic similarity, exist between the models if the ratios of the forces acting at the corresponding points in them have the same magnitude with parallel directions. In functional forms, the dimensional analysis of a relative motion problem of a real spacecraft can be described in terms of a set of non-dimensional parameters π terms as

$$(\pi)_{real} = f\left\{(\pi_1)_{real}, (\pi_2)_{real}, (\pi_3)_{real}, ..., (\pi_{n-k})_{real}\right\} \tag{29}$$

while that of the scaled spacecraft model, governed by the same variables and having the same behavior as the real spacecraft, can be written as

$$(\pi)_{scaled} = f\left\{(\pi_1)_{scaled}, (\pi_2)_{scaled}, (\pi_3)_{scaled}, ..., (\pi_{n-k})_{scaled}\right\} \tag{30}$$

By the similarity principle, with the scaled and real model having the same phenomenon, Eqs. (29) and (30) are the same. Therefore, the prediction equation is $(\pi)_{real} = (\pi)_{scaled}$ gives

$$(\pi_1)_{real} = (\pi_1)_{scaled}, (\pi_2)_{real} = (\pi_2)_{scaled}, (\pi_3)_{real} = (\pi_3)_{scaled}, ..., (\pi_{n-k})_{real} = (\pi_{n-k})_{scaled} \tag{31}$$

Eq. (31) shows that the values measured by the scaled spacecraft model are corresponding to those of the real spacecraft model.

Development of the Scaling Laws for Scaled Relative Motion Dynamics

This section summarizes the scaling laws derived in References 16 and 17. The planar relative motion dynamics in radial (x) and along-track (y) directions, with the presence of thrust forces F_x and F_y,can be expressed as

$$\begin{aligned} \ddot{x} - 2\omega\dot{y} - 3\omega^2 x &= \frac{F_x}{m} \\ \ddot{y} + 2\omega\dot{x} &= \frac{F_y}{m} \end{aligned} \tag{32}$$

where m is the spacecraft mass. Eq. (32) has eleven n variables t, x, y, $\dot{x}$, $\dot{y}$, $\ddot{x}$, $\ddot{y}$, F_x, F_y, m, ω and three primary k variables M, L and T making eight p, π parameters. Each of the p variables has the following dimensional formula

$$\begin{gathered} t = [T], m = [M], x, y = [L], \omega = \left[T^{-1}\right], \dot{x}, \dot{y} = \left[LT^{-1}\right], \\ \ddot{x}, \ddot{y} = \left[LT^{-2}\right], F_x = F_y = \left[MLT^{-2}\right] \end{gathered} \tag{33}$$

Choosing t, x and m as fundamental k variables we have the π parameters

$$\begin{gathered} (\pi_1)_{real} = t^{a_1} x^{a_2} m^{a_3} y, \quad (\pi_2)_{real} = t^{a_4} x^{a_5} m^{a_6} \dot{x}, \quad (\pi_3)_{real} = t^{a_7} x^{a_8} m^{a_9} \dot{y}, \\ (\pi_4)_{real} = t^{a_{10}} x^{a_{11}} m^{a_{12}} \ddot{x}, \quad (\pi_5)_{real} = t^{a_{13}} x^{a_{14}} m^{a_{15}} \ddot{y}, \quad (\pi_6)_{real} = t^{a_{16}} x^{a_{17}} m^{a_{18}} F_x, \\ (\pi_7)_{real} = t^{a_{19}} x^{a_{20}} m^{a_{21}} F_y, (\pi_8)_{real} = t^{a_{22}} x^{a_{23}} m^{a_{24}} \omega \end{gathered} \tag{34}$$

where, $a_1, ..., a_{24}$ are the unknown exponents which can be determined by assuming that each of the π parameters is dimensionless.

The scaled relative motion dynamics

$$\begin{aligned} \ddot{\tilde{x}} - 2\tilde{\omega}\dot{\tilde{y}} - 3\tilde{\omega}^2\tilde{x} &= \frac{\tilde{F}_{\tilde{x}}}{\tilde{m}} \\ \ddot{\tilde{y}} + 2\tilde{\omega}\dot{\tilde{x}} &= \frac{\tilde{F}_{\tilde{y}}}{\tilde{m}} \end{aligned} \tag{35}$$

has eleven $\tilde{n}$ variables $\tilde{t}$, $\tilde{x}$, $\tilde{y}$, $\dot{\tilde{x}}$, $\dot{\tilde{y}}$, $\ddot{\tilde{y}}$, $\ddot{\tilde{y}}$, $\tilde{F}_{\tilde{x}}$, $\tilde{F}_{\tilde{y}}$, $\tilde{m}$, $\tilde{\omega}$, three $\tilde{k}$ variables and eight $\tilde{p}$ variables. In a similar manner, as Eq. (34) was derived, the scaled model π-parameters are

$$\begin{gathered} (\pi_1)_{scaled} = \tilde{t}^{b_1} \tilde{x}^{b_2} \tilde{m}^{b_3} \tilde{y}, \quad (\pi_2)_{scaled} = \tilde{t}^{b_4} \tilde{x}^{b_5} \tilde{m}^{b_6} \dot{\tilde{x}}, \quad (\pi_3)_{scaled} = \tilde{t}^{b_7} \tilde{x}^{b_8} \tilde{m}^{b_9} \dot{\tilde{y}}, \\ (\pi_4)_{scaled} = \tilde{t}^{b_{10}} \tilde{x}^{b_{11}} m^{b_{12}} \ddot{\tilde{x}}, \quad (\pi_5)_{scaled} = \tilde{t}^{b_{13}} \tilde{x}^{b_{14}} \tilde{m}^{b_{15}} \ddot{\tilde{y}}, \quad (\pi_6)_{scaled} = \tilde{t}^{b_{16}} \tilde{x}^{b_{17}} \tilde{m}^{b_{18}} \tilde{F}_{\tilde{x}}, \\ (\pi_7)_{scaled} = \tilde{t}^{b_{19}} \tilde{x}^{b_{20}} \tilde{m}^{b_{21}} \tilde{F}_{\tilde{y}}, (\pi_8)_{scaled} = \tilde{t}^{b_{22}} \tilde{x}^{b_{23}} \tilde{m}^{b_{24}} \tilde{\omega} \end{gathered} \tag{36}$$

Non-dimensionalizing the first π-parameters in Eqs. (34) and (36) we have

$$\begin{aligned} (\pi_1)_{real} &= T^0 L^0 M^0 = T^{a_1} L^{a_2} M^{a_3} L = T^{a_1} L^{a_2+1} M^{a_3} \\ (\pi_1)_{scaled} &= T^0 L^0 M^0 = T^{b_1} L^{b_2} M^{b_3} L = T^{b_1} L^{b_2+1} M^{b_3} \end{aligned} \tag{37}$$

Equating the powers of the primary dimensions we have

$$a_1 = 0, a_2 = -1, a_3 = 0, b_1 = 0, b_2 = -1, b_3 = 0 \tag{38}$$

Table 1. π-parameters of the real and scaled spacecraft.

π-parameters	Real Spacecraft	Scaled Spacecraft
π_1	$x^{-1}y$	$\tilde{x}^{-1}\tilde{y}$
π_2	$tx^{-1}\dot{x}$	$\tilde{t}\tilde{x}^{-1}\dot{\tilde{x}}$
π_3	$tx^{-1}\dot{y}$	$\tilde{t}\tilde{x}^{-1}\dot{\tilde{y}}$
π_4	$t^2x^{-1}\ddot{x}$	$\tilde{t}^2\tilde{x}^{-1}\ddot{\tilde{x}}$
π_5	$t^2x^{-1}\ddot{y}$	$\tilde{t}^2\tilde{x}^{-1}\ddot{\tilde{y}}$
π_6	$t^2x^{-1}m^{-1}F_x$	$\tilde{t}^2\tilde{x}^{-1}\tilde{m}^{-1}\tilde{F}_{\tilde{x}}$
π_7	$t^2x^{-1}m^{-1}F_y$	$\tilde{t}^2\tilde{x}^{-1}\tilde{m}^{-1}\tilde{F}_{\tilde{y}}$
π_8	$t^2x^{-1}m^{-1}\omega$	$\tilde{t}^2\tilde{x}^{-1}\tilde{m}^{-1}\tilde{\omega}$

Therefore, the first π parameter for both real and scaled spacecraft can be written as

$$(\pi_1)_{scaled} = x^{-1}y, \qquad (\pi_1)_{scaled} = \tilde{x}^{-1}\tilde{y} \tag{39}$$

Using the same approach the remaining π-parameters are calculated and the results are shown in Table 1. Application of the similarity principle in Eq. (31) gives the following scaling laws

$$\begin{array}{lllllll} x = \tilde{x}\lambda_x, & \lambda_{\dot{x}}\lambda_t = \lambda_x, & \lambda_{\ddot{x}}\lambda_t^2 = \lambda_x, & \lambda_{F_x}\lambda_t^2 = \lambda_m\lambda_x, & t = \tilde{t}\lambda_t, & \lambda_\omega\lambda_t = 1 \\ y = \tilde{y}\lambda_y, & \lambda_{\dot{y}}\lambda_t = \lambda_y, & \lambda_{\ddot{y}}\lambda_t^2 = \lambda_y, & \lambda_{F_y}\lambda_t^2 = \lambda_m\lambda_y, & m = \tilde{m}\lambda_m & \end{array} \tag{40}$$

The laws are used to scale the real spacecraft orbital dynamics to that of the FSS.

DESIGN OF TIP-TILT HARDWARE-IN-THE-LOOP AIR-BEARING TESTBED

In this section, the design and development of Tip-Tilt Hardware-in-the-Loop testbed for the purpose of physically emulating the relative motion dynamics is presented. The testbed is made up of a Floating Spacecraft Simulator, granite table ($8' \times 6'$), a PC-Controller, two actuators, two servo motors and servo drive.

Tip-Tilt HIL Testbed Design Methodology

The systematic approach followed to achieve the Tip-Tilt HIL project is shown in Figure 4. The design methodology is divided into three main parts: Floating Spacecraft Simulator dynamics, Steering logic and Actuation strategy.

The first part contains the scaled HCW dynamics, shown in Eq. (35), and from which the scaled relative position and velocity are obtained. The second part, that is the steering logic, produces the mathematical model of the displacement height. The output of the first part is scaled up, using the scaling laws developed in Eq. (40) and then passed into the desired spacecraft HCW dynamics and then scaled down. Afterward the scaled down acceleration, acceleration due to gravity and the developed system matrix in Eq. (27) are used to formulate the two screw height displacements which are converted into the revolutions and pulses used by the controllers 1 and 2 to operate the two mechanical screw actuators.

The schematic representation of the practical approach of the Tip-Tilt HIL testbed is shown in Figure 5 and FSS is shown in Figure 6. The HTC VIVE tracker attached to the FSS communicates

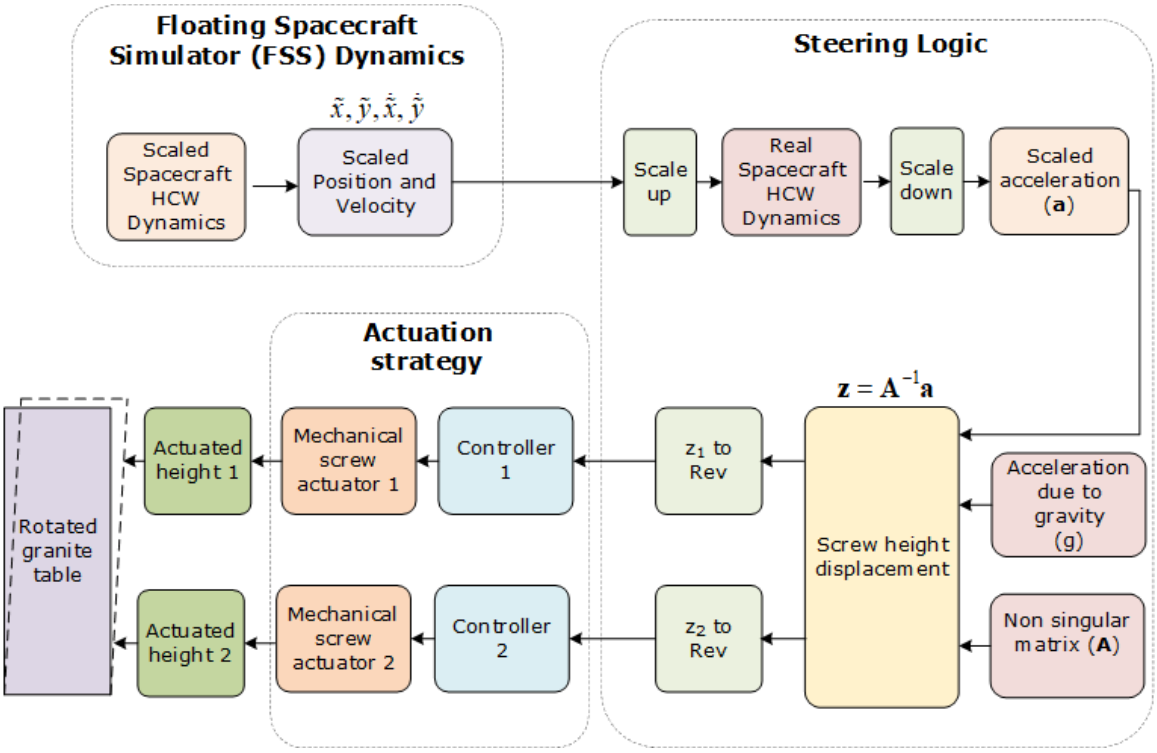

Figure 4. Tip-Tilt HIL Testbed Design Methodology.

wirelessly with the VIVE dongle, connected to one of the PC controller's USB ports, which in-turn transmits tracking data (inform of position, linear velocity, angular velocity and attitude of the FSS) to the PC controller. The controller sends control command to the FSS to carry out maneuver and to emulate the relative orbital dynamics. After sending actuation command signal to the two controllers, in charge of controlling the mechanical screw actuator, the granite table is tilted in response thereby dynamically changing the inclination which in effect will aid the physical emulation of the relative motion.

AC Motor and Servo Drives

The AC motor and servo drives of AutomationDirect are selected for the testbed development. The two SureServo brushless motors, model number SVM-210, have the following characteristics: integrated encoder with 2,500 (x4) pulses/revolution plus marker pulse (once per revolution), optional 24 VDC spring-set holding brakes, standard hook-up cables for motor power/brake and encoder and standard DIN-rail mounted ZIPLink break-out kit for the drive CN1 connector (with screw terminal connections).

The servo drives can be configured for a wide range of command sources including analog torque, analog velocity, step and direction or up and down pulse position, quadrature encoder follower, and built-in motion controller with preset position, velocity, or torque. Presets can be selected with discrete inputs or modified with the MODBUS serial interface. The servo drive is a fully digital system with up to 450 Hz velocity loop response. Configuration and diagnostics of the servo drives can be accomplished with the integrated keypad/display or the easy-to-use SureServo Pro software on a Windows environment. A PC controller is used to communicate with the Floating Spacecraft

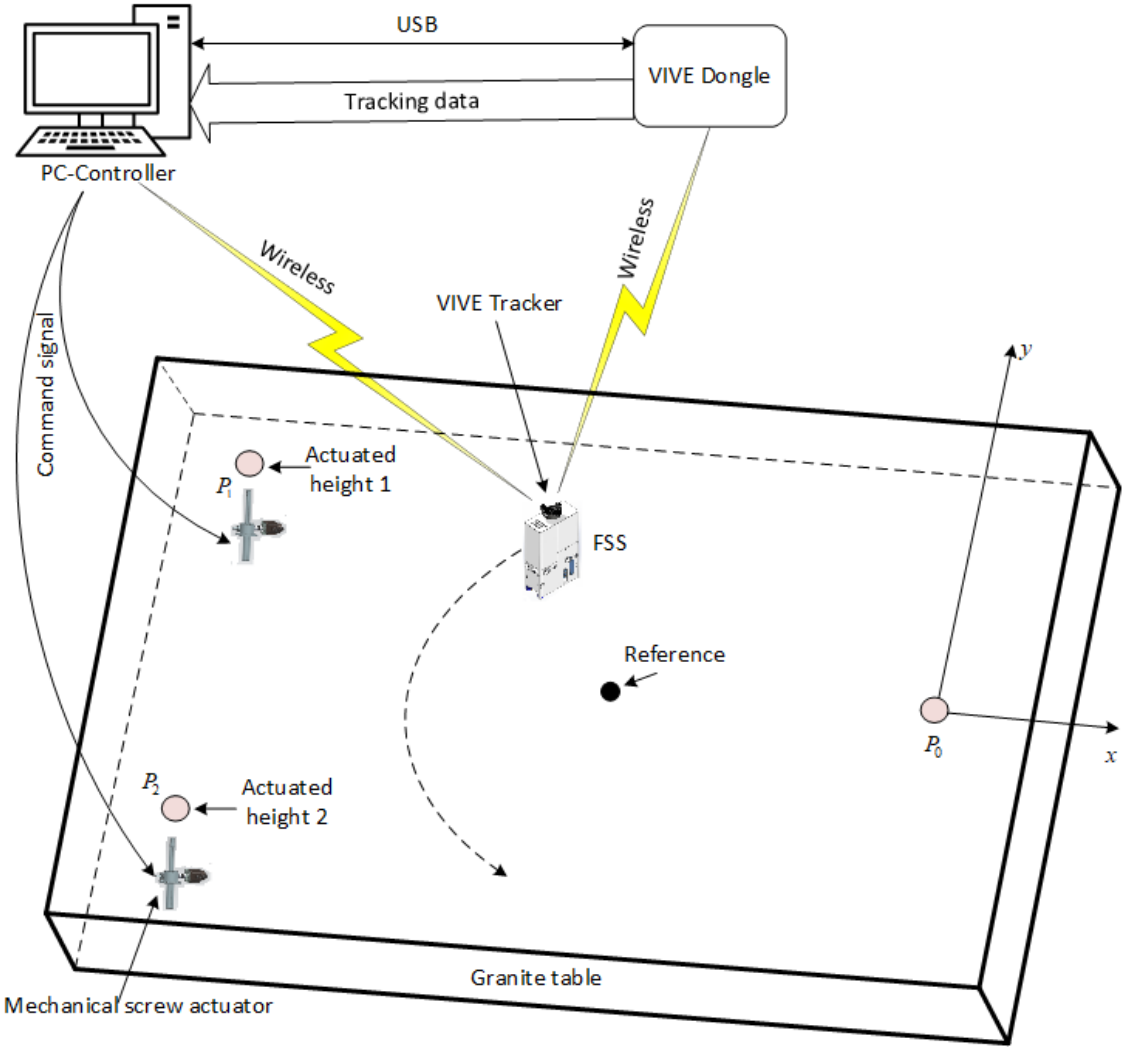

Figure 5. Schematic Representation of the Practical Approach of Tip-Tilt HIL Testbed.

Simulator, with the motor and the actuators. The communication is done using MATLAB/Simulink software.

CAD Models of Tip-Tilt Testbed

The integration of the individual components of Tip-Tilt HIL testbed using SIEMENS NX software and the actual granite table model are shown in Figure 6. The CAD models allow us to create a complete digital prototype and better understanding of the system. The Tip-Tilt HIL system arrangement includes two actuator systems each connected to a separate motor, two couplers to connect the motor shaft to the actuator shaft and supporting beam. Each of the machine screw actuators has an inbuilt gearbox. The materials acquired for the project are shown in Figure 7.

NUMERICAL SIMULATIONS OF THE PHYSICAL EMULATION OF THE RELATIVE MOTION DYNAMICS BY THE SCALED FLOATING SPACECRAFT SIMULATOR

The applicability of the new idea is demonstrated using spacecraft of mass 1000 kg in a Low Earth Orbit (LEO) of altitudes 400 km. The spacecraft has mean motion of $n = 0.0011$ rad/s. The scaled down planar dynamics of Hill-Clohessy-Wilshire (HCW) recreated by the FSS of mass 3.585 kg and dimension of $0.10 \times 0.226 \times 0.366$ m is simulated and presented. Table 2 shows mass, time and initial conditions of the circumnavigation scenario while Table 3 shows the parameters of the emulated motion on the granite table. Using Eq. (40), the scaling parameters obtained are shown in Tables 4 and 5. The two successive rotations of the mechanical screw actuators, which inturn caused the testbed to be dynamically tilted, created external disturbance force

$$\begin{aligned} \tilde{F}_x &= g\left(\frac{y_2 z_1}{l_2 d_1} + \frac{y_1 z_2}{l_1 d_2}\right) \\ \tilde{F}_y &= -g\left(\frac{x_2 z_1}{l_2 d_1} + \frac{x_1 z_2}{l_1 d_2}\right) \end{aligned} \tag{41}$$

The disturbance force mimicks the disturbance experienced by a real spacecraft in orbit. Upon substitution of the coordinates (-1.3208, 0.508) m and (-1.3208,-0.508) m of the two MSAs at points P_1 and P_2 we obtain the non-singular matrix $\mathbf{A}$, shown in Eq. (27), as

$$\mathbf{A} = \begin{bmatrix} 0.3786 & -0.3786 \\ -0.9843 & -0.9843 \end{bmatrix} \tag{42}$$

Table 2. Orbiting spacecraft mass, time and initial conditions of three cases of circumnavigation.

Spacecraft mass, kg	Time, t_f, s	x_0, m	y_0, m	$\dot{x}_0$, m/s	$\dot{y}_0$, m/s
1000	5.5535e+03	0	100	0.1	0

The orbiting spacecraft x, y and acceleration trajectories, without the effects of external disturbances, are shown in Figure 8. The scaled emulated x, y, acceleration, forcing term and screw height displacements trajectories at different instant of time are shown in Figures 9 and 10. Circumnavigation on dynamically tilted granite table is shown in Fig 11. Closer examination of the three cases of circumnavigation considered showed that the new idea of dynamically tilting the table gave better results than just maneuvering the FSS on a planar operating surface. This is evidence on the emulated scaled relative motion of the Floating Spacecraft Simulator.

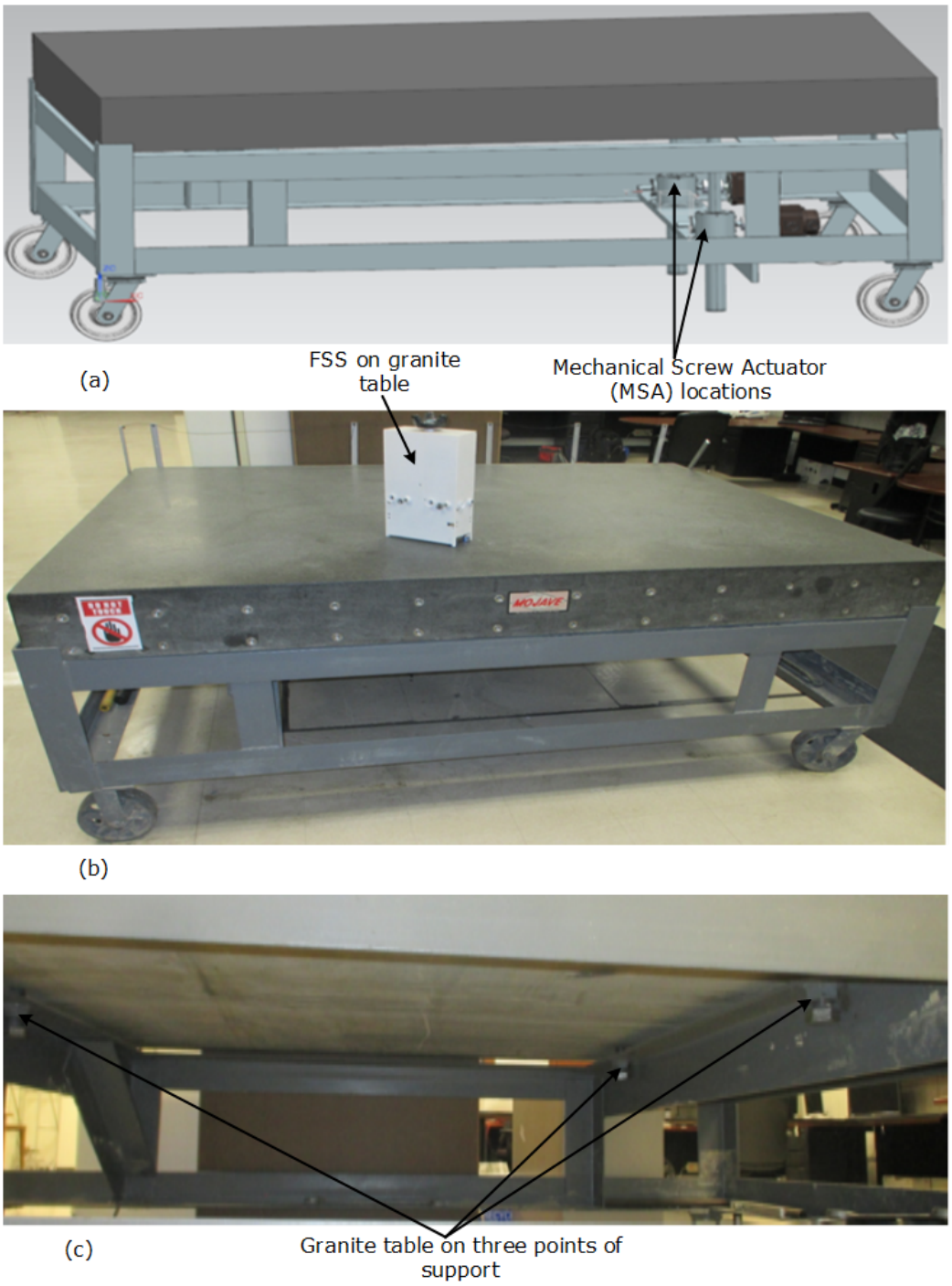

Figure 6. Granite table model (a) 3D model with MSA supports, (b) $8' \times 6'$ granite table (c) Bolt support points before modification

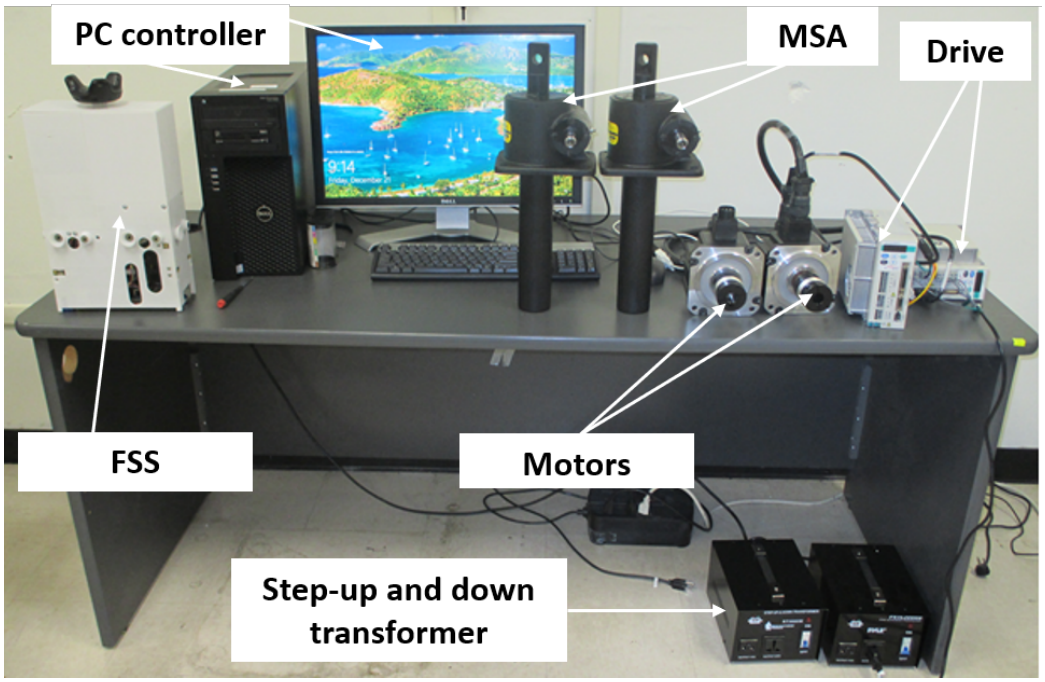

Figure 7. Project materials.

Table 3. Emulated motion on the granite table.

Simulator mass, kg	Time, $\tilde{t}_f$, s	$\tilde{x}_0$, m	$\tilde{y}_0$, m	$\dot{\tilde{x}}_0$, m/s	$\dot{\tilde{y}}_0$, m/s
3.585	60	0	0.1	1e-05	0

Table 4. Scaling parameters of three different cases of circumnavigation.

λ_x	λ_y	$\lambda_{\dot{x}}$	$\lambda_{\dot{y}}$	$\lambda_{\ddot{x}}$	$\lambda_{\ddot{y}}$
$1e+03$	$1e+03$	$1e+04$	$1e+04$	0.1167	0.1167

Table 5. Scaling parameters of three different cases of circumnavigation.

λ_t	λ_m	λ_ω	λ_{F_x}	λ_{F_y}
92.5605	278.9400	0.0108	32.5582	32.5582

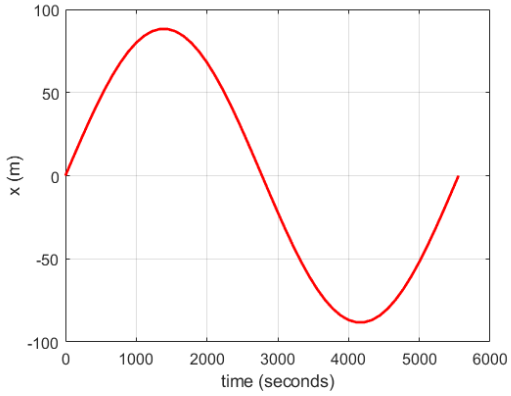

(a) Radial trajectories

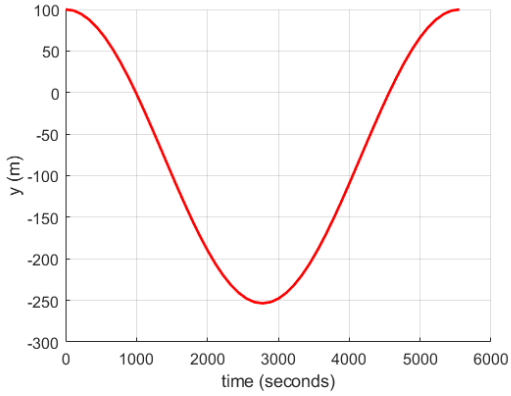

(b) Along-track trajectories

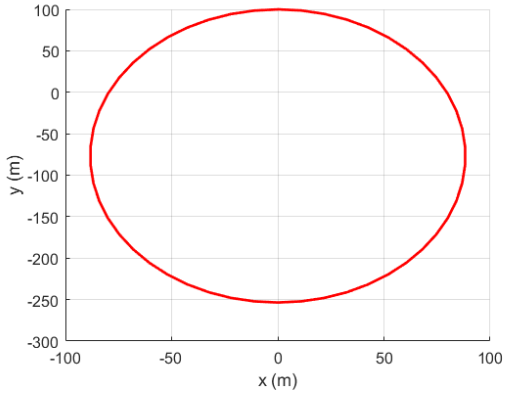

(c) Along-track/radial trajectories

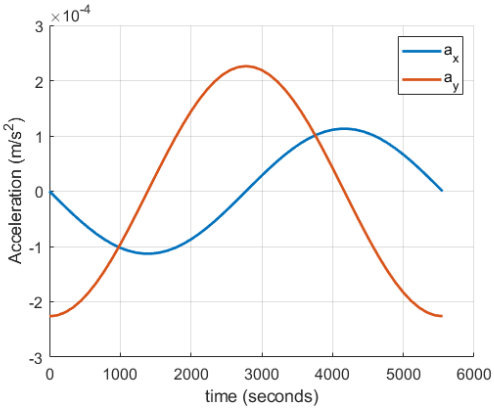

(d) Acceleration trajectories

Figure 8. Orbiting spacecraft trajectories

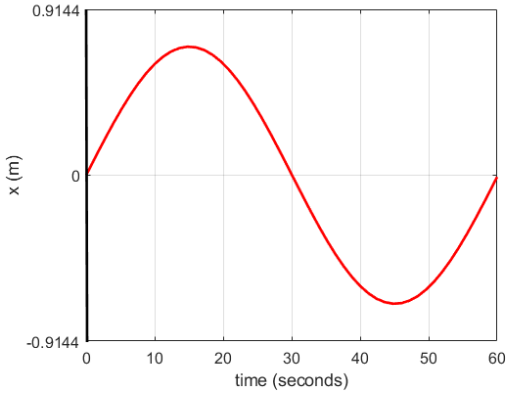

(a) Scaled radial trajectories

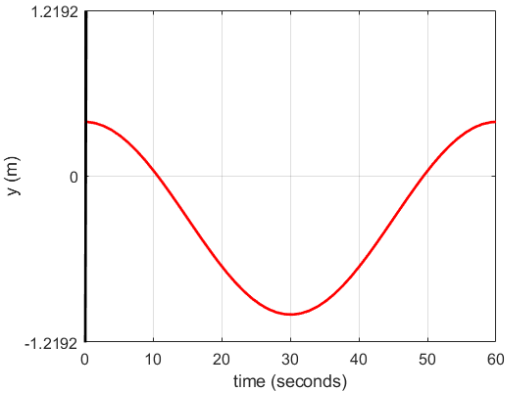

(b) Scaled along-track trajectories

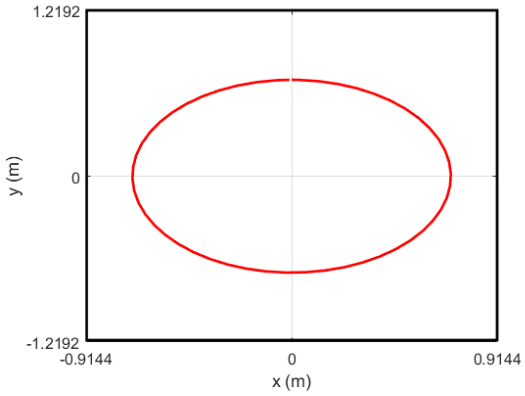

(c) Scaled along-track/radial trajectories

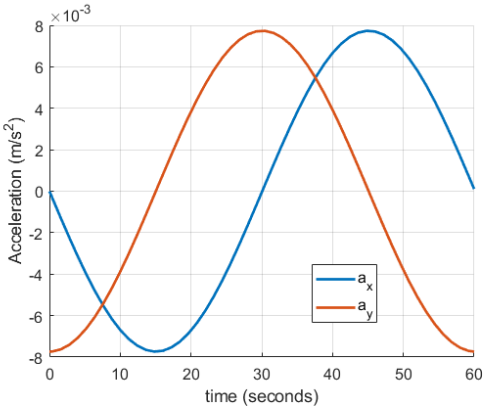

(d) Scaled acceleration trajectories

Figure 9. Emulated motion of FSS on the granite table

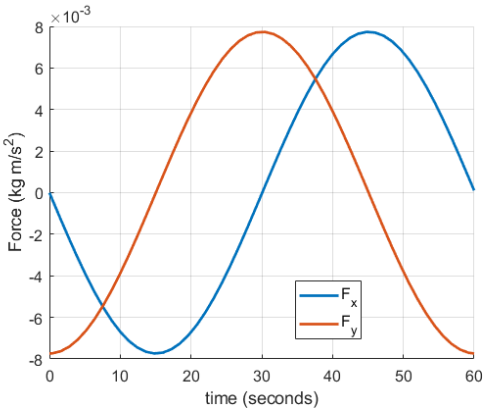

(a) Force due to dynamical tilting of the table

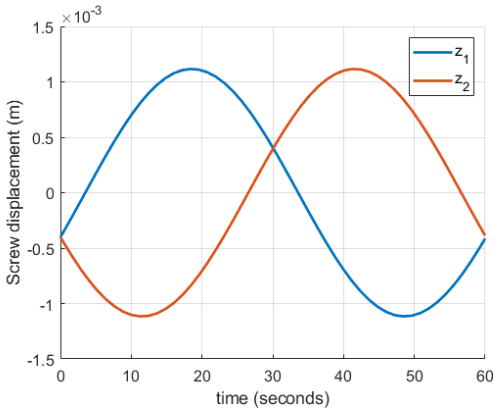

(b) Displacement due to two successive rotations

Figure 10. Force and screw height displacement

CONCLUSION

The design and development of a new hardware-in-the-loop air bearing testbed that has the ability to physically emulate the relative orbital dynamics of a deputy spacecraft with respect to the chief spacecraft has been presented. The air-bearing testbeds widely adopted are limited to reproduce short maneuvers. Using the current approach the applicability of the airbearing testbeds are extended to the recreation of relative orbital dynamics by dynamically tilting the operating surface so that longer maneuvers can be emulated. Using Euler's rotation theorem, the mathematical constructs of the mechanical screw actuators height displacements and the tilt angles are obtained. The scaling factors of the relative motion dynamics of the scaled spacecraft model (FSS) is developed via Buckingham's Pi theorem and similarity principle. The similarities between the scaled and the real spacecraft models are established after the determination of the π groups. Through numerical simulations the suitability of the new idea is demonstrated. The presented circumnavigation maneuver scenario show that, after dynamically tilting the operating surface, the new approach gave a better representation of the relative motion dynamics.

REFERENCES

[1] H. K. Fathy, Z. S. Filipi, J. Hagena, and J. L. Stein, "Review of Hardware-in-the-Loop Simulation and Its Prospects in the Automotive Area," *Proc. of SPIE*, 2006, pp. 1–20.

[2] H. Schaub, S. R. Vadali, J. L. Junkins, and K. T. Alfriend, "Spacecraft Formation Flying Control using Mean Orbit Elements," *Journal of the Astronautical Sciences*, Vol. 48, 2000, p. 6987.

[3] F. Flechtner, P. Morton, M. Watkins, and F. Webb, "Status of the grace follow-on mission, Gravity, Geoid and Height Systems," *Springer*, 2014, p. 117121.

[4] G. Krieger, M. Zink, M. Bachmann, B. Brutigam, D. Schulze, M. Martone, P. Rizzoli, U. Steinbrecher, J. Antony, F. D. Zan, and e. al., "Tandem-x: a radar interferometer with two formation-flying satellites," *Acta Astronaut.*, Vol. 89, 2013, p. 8398.

[5] K. Danzmann, "Lisa mission overview," *Adv. Space Res.*, Vol. 25, 2000, p. 11291136.

[6] S. G. Ungar, J. S. Pearlman, J. A. Mendenhall, and D. Reuter, "Overview of the earth observing one (eo-1) mission," *IEEE Trans. Geosci. Rem. Sens.*, Vol. 41, 2003, p. 11491159.

[7] G. Hill, "Researches in lunar theory," *American Journal of Mathematics*, 1878, pp. 5–26.

[8] W. H. Clohessy and R. S. Wiltshire, "Terminal guidance system for satellite rendezvous," *Journal of the Aerospace Sciences*, Vol. 27, 1960, pp. 653–658.

[9] J. Leitner, "A Hardware-in-the-Loop Testbed for Spacecraft Formation Flying Applications," *Proceedings of the IEEE Aerospace Conference*, 2001, p. 2/6152/620.

[10] D. Scharf, F. Hadaegh, J. Keim, E. Benowitz, and P. Lawson, "Flight-like ground demonstration of precision formation flying spacecraft," *Proc. SPIE*, 2007, p. 669307.

[11] H. Daitx, M. Schlotterer, J. Whidborne, and M. Sagliano, "Development of a combined attitude and position controller for a satellite simulator," *67th International Astronautical Congress (IAC)*, 2006.

[12] R. Zappulla, J. Virgili-Llop, C. Zagaris, H. Park, and M. Romano, "Dynamic air-bearing hardware-in-the-loop testbed to experimentally evaluate autonomous spacecraft proximity maneuvers," *J. Spacecraft Rockets*, Vol. 54, 2017, p. 825839.

[13] K. Saulnier, D. Prez, R. Huang, D. Gallardo, G. Tilton, and R. Bevilacqua, "A six-degree-of-freedom hardware-in-the-loop simulator for small spacecraft," *Acta Astronaut.*, Vol. 105, 2014, p. 444462.

[14] P. Tsiotras, "Astros: a 5dof experimental platform for research in spacecraft proximity operations," *AAS Guidance and Control Conference*, 2014.

[15] Y. Eun, S. Park, and G. Kim, "Development of a hardware-in-the-loop testbed to demonstrate multiple spacecraft operations in proximity," *Acta Astronautica*, Vol. 147, 2018, pp. 48–58.

[16] J. VirgiliLlop, R. Zappulla-II, and M. Romano, "Dynamically tilting flat table to impart a time-varying gravity-induced acceleration on a floating spacecraft simulator," *Patent Pending 62 455 775*, 2017, pp. 1–46.

[17] M. Ciarcia, R. Cristi, and M. Romano, "Emulating Scaled Clohessy–Wiltshire Dynamics on an Air-Bearing Spacecraft Simulation Testbed," *Journal of Guidance, Control, and Dynamics*, Vol. 40, No. 10, 2017, pp. 2496–2510, 10.2514/1.G002585.

[18] P. C. Hughes, *Spacecraft Attitude Dynamics*. Dover Publications, Inc., Mineola, New York, 2004.

[19] B. C. Wang, E. Yee, and D. Bergstrom, "Development of a hardware-in-the-loop testbed to demonstrate multiple spacecraft operations in proximityGeometrical description of subgridscale stress tensor based on Euler axis/angle," *AIAA J.*, Vol. 44, 2006, p. 11061110.

[20] E. Buckingham, "On physically similar systems; illustrations of the use of dimensional equations," *Physical Review*, Vol. 4, 1914, pp. 345–376.

[21] E. Buckingham, "Model Experiments and the Form of Empirical Equations," *Trans. ASME*, Vol. 37, 1915, p. 263.